0026-895X/10/7705-784–792
MOLECULAR PHARMACOLOGY
U.S. Government work not protected by U.S. copyright
Mol Pharmacol 77:784–792, 2010

Vol. 77, No. 5
61424/3580698
Printed in U.S.A.

Inhibitor of κB Kinase β Regulates Redox Homeostasis by Controlling the Constitutive Levels of Glutathione[S]

Zhimin Peng, Esmond Geh, Liang Chen, Qinghang Meng, Yunxia Fan, Maureen Sartor, Howard G. Shertzer, Zheng-Gang Liu, Alvaro Puga, and Ying Xia

Department of Environmental Health and Center of Environmental Genetics, University of Cincinnati Medical Center, Cincinnati, Ohio (Z.P., E.G., L.C., Q.M., Y.F., M.S., H.G.S., A.P., Y.X.); and Cell and Cancer Biology Branch, Center for Cancer Research, National Cancer Institute, National Institutes of Health, Bethesda, Maryland (Z.G.L.)

Received October 1, 2009; accepted February 12, 2010

ABSTRACT

Cytokine-activated inhibitor of κB kinase β (IKKβ) is a key mediator of immune and inflammatory responses, but recent studies suggest that IKKβ is also required for tissue homeostasis in physiopathological processes. Here we report a novel role for IKKβ in maintenance of constitutive levels of the redox scavenger GSH. Inactivation of IKKβ by genetic or pharmacological means results in low cellular GSH content and marked reduction of redox potential. Similar to *Ikkβ*(−/−) cells, *Tnfr1*(−/−) and *p65*(−/−) cells are also GSH-deficient. As a consequence, cells deficient in IKKβ signaling are extremely susceptible to toxicity caused by environmental and pharmacological agents, including oxidants, genotoxic agents, microtubule toxins, and arsenic. GSH biosynthesis depends on the activity of the rate-limiting enzyme glutamate-cysteine ligase (GCL), consisting of a catalytic subunit (GCLC) and a modifier subunit (GCLM). We found that loss of IKKβ signaling significantly reduces basal NF-κB activity and decreases binding of NF-κB to the promoters of *Gclc* and *Gclm*, leading to reduction of GCLC and GCLM expression. Conversely, overexpression of GCLC and GCLM in IKKβ-null cells partially restores GSH content and prevents stress-induced cytotoxicity. We suggest that maintenance of GSH is a novel physiological role of the IKKβ-NF-κB signaling cascade to prevent oxidative damage and preserve the functional integrity of the cells.

The nuclear factor-κB (NF-κB) is a stimulus-activated transcription factor involved in the control of fundamental cellular processes, such as proliferation, apoptosis, and differentiation (Pahl, 1999). NF-κB is normally sequestered by IκBα as an inactive complex in the cytosol but activated by growth factors and inflammatory cytokines, such as TNFα. TNFα binds to its receptor and activates a receptor-associated signalsome, composed of TRADD, TRAF2/5, RIP, and MAP3Ks. The receptor complex in turn activates IKKβ, which phosphorylates IκBα followed by IκBα ubiquitylation and proteosome-dependent degradation. Subsequently, NF-κB is released from IκBα and translocates to the nucleus, where it binds to consensus NF-κB sites in DNA to activate gene expression (Pahl, 1999). Through binding to its target DNA, widely distributed in the genome, NF-κB participates in the regulation of a vast number of genes and diverse cell activities.

Cytokine-induced activation of the IKK–NF-κB cascade is best known for its roles in innate immunity and inflammatory responses, but emerging evidence indicates that this pathway is required for the modulation of stress responses. In vitro studies show that cells deficient in IKKβ, IKKβ upstream TRAF2 and TRAF5, or downstream NF-κB RelA/

This work was supported in part by the National Institutes of Health National Institute of Environmental Health Sciences [Grants ES11798, ES10708, ES06096, T32-ES007250]; by the National Institutes of Health National Eye Institute [Grant EY15227]; and by Intramural Research Program of the National Institutes of Health National Cancer Institute.

Article, publication date, and citation information can be found at http://molpharm.aspetjournals.org.

doi:10.1124/mol.109.061424.

[S] The online version of this article (available at http://molpharm.aspetjournals.org) contains supplemental material.

ABBREVIATIONS: NF-κB, nuclear factor-κB; IκBα, inhibitor of κB; TNFα, tumor necrosis factor; TNFR, tumor necrosis factor receptor; TRAF, TNFR-associated factor; IKK, IκB kinase; ROS, reactive oxygen species; GCL, glutamate cysteine ligase; GCLC, glutamine cysteine ligase catalytic subunit; GCLM, glutamine cysteine ligase modifier subunit; AP-1, activator protein-1; NRF2, NF-E2-related factor-2; JSH23, 4-methyl-N^1-(3-phenylpropyl)benzene-1,2-diamine; BMS-345541, 4-(2′-aminoethyl)amino-1,8-dimethylimidazo[1,2-*a*]quinoxaline; TPCA-1, [5-(*p*-fluorophenyl)-2-ureido]thiophene-3-carboxamide; luminol, 5-amino-2,3-dihydro-1,4-phthalazinedione; DMEM, Dulbecco's modified Eagle's medium; FBS, fetal bovine serum; DTPA, diethylenetriaminepenta-acetic acid; DCFDA, 2′,7′-dichlorofluorescin-diacetate; PBS, phosphate-buffered saline; DAPI, 4,6-diamidino-2-phenylindole; KRB, KCl-respiratory buffer; TUNEL, terminal deoxynucleotidyl transferase dUTP nick-end labeling; MTT, 3-(4,5-dimethylthiazol-2-yl)-2,5-diphenyltetrazolium bromide; PCR, polymerase chain reaction; siRNA, small interfering RNA; ChIP, chromatin immunoprecipitation; kbp, kilobase pair(s); RT-PCR, reverse transcription-polymerase chain reaction; IgG, immunoglobulin G.

p65 subunit, have reactive oxygen species (ROS) accumulation and are extremely sensitive to apoptosis in response to toxic compounds and stress inducers (Cosulich et al., 2000; Chen et al., 2003; Sakon et al., 2003; Kamata et al., 2005; Peng et al., 2007). In vivo, hepatocyte-specific IKKβ deficient mice show reduced antioxidant expression and excessive ROS in the liver in response to diethylnitrosamine (DEN), which is metabolized into an alkylating agent that induces oxidative stresses and causes DNA damage. The ROS in turn lead to sustained activation of c-Jun N-terminal kinases and increased liver cell death (Boitier et al., 1995; Maeda et al., 2005). Together, these observations suggest that the classic IKKβ-NF-κB pathway may help to maintain cellular redox potential and prevent oxidative stress.

The thiol group-containing tripeptide L-γ-glutamyl-L-cysteinyl-L-glycine (i.e., GSH) is a prominent intracellular antioxidant responsible for hydrophilic scavenging of radicals and for maintaining the redox state of proteins. In most cell types, GSH plays a major role in protecting cells against toxicity arising from environmental stresses (Meister and Anderson, 1983). GSH level is primarily determined by its de novo synthesis, carried out by the consecutive action of the two ATP-dependent enzymes glutamate cysteine ligase (GCL) and GSH synthase (Meister and Anderson, 1983). GCL is a holoenzyme, consisting of a catalytic subunit (GCLC) and a regulatory subunit (GCLM) and acts as the rate-limiting enzyme for GSH biosynthesis. Many oxidative stress and abnormal growth conditions can induce GCLC and GCLM expression, resulting in elevated GCL activity and GSH levels. In these cases, the elevated GSH serves as a natural defense mechanism for cells to fight against stress conditions (Lu, 2009). In addition to detoxification, GSH also participates in maintaining physiological homeostasis and balance of the biological systems, whereas its deficiency is associated with a wide range of pathological conditions, including cancer, neurological disorders and rapid aging (Townsend et al., 2003).

A number of stress-activated transcription factors, such as AP-1, NRF2, and NF-κB, are involved in the regulation of *Gclc* and *Gclm* at the level of gene transcription (Sierra-Rivera et al., 1994; Lu, 2009). NF-κB has been shown to bind directly to and activate the *Gclc* promoter, whereas it indirectly regulates the *Gclm* promoter by activating AP-1 (Yang et al., 2005b). A dominant-negative NF-κB blocks basal and TNFα-induced expression of GCLC and GCLM, but the intracellular signaling pathways responsible for GSH homeostasis have not been further characterized. That has been the objective of the present studies, in which we show that regulation of the basal levels of GCLC and GCLM expression and GSH homeostasis in unstressed cells is the consequence of IKKβ signals required to maintain a basal level of NF-κB activity in the absence of inducers. Inactivation of this pathway markedly reduces cellular GSH and sensitizes cells to cytotoxicity in response to stress stimuli.

Materials and Methods

Reagents, Antibodies, Plasmids and Cell Culture Conditions. The chemical inhibitors of IKKβ and NF-κB and the concentrations at which they were used are as follows: 10 μM JSH23, 1 μM BMS-345541, and 0.5 μM TPCA-1, all from Calbiochem-Novabiochem (San Diego, CA. Antibodies to β-actin were from BD Biosciences Pharmingen (San Diego, CA); those to phospho-p65, p65, and p50 were from Santa Cruz Biotechnology (Santa Cruz, CA); and anti-GCLC and anti-GCLM were a gift from Dr. Ying Chen (University of Cincinnati, Cincinnati, OH). Sodium arsenite, luminol (5-amino-2,3-dihydro-1,4-phthalazinedione), horseradish peroxidase, catalase, GSH, and GSSG were from Sigma (St. Louis, MO), and TNFα was from PeproTech (Rocky Hill, NJ).

Luciferase reporter plasmids containing binding elements for NF-κB (NF-κB-luc) (Tojima et al., 2000), AP-1 (AP1-luc), NRF2 (Nqo1-luc) (Hoffer et al., 1996), and the *Gclm* (*Gclm*-luc) (Yang et al., 2005b) and *Gclc* (*Gclc*-luc) promoter-driven luciferase plasmids are described elsewhere. The expression vectors for β-galactosidase were from commercial sources (Thermo Fisher Scientific, Waltham, MA), and those for murine GCLC and GCLM were a gift from Dr. Tim Dalton (University of Cincinnati, Cincinnati, OH). The siGENOME SMARTpool siRNA for mouse *Ikkβ* were from Dharmacon/Thermo Fisher Scientific (Lafayette, CO).

All cell culture reagents, including Dulbecco's modified Eagle's medium (DMEM), fetal bovine serum (FBS), L-glutamine, minimal essential medium nonessential amino acids, penicillin-streptomycin, and minimal essential medium vitamins were from Invitrogen (Carlsbad, CA). The wild-type, IKKβ-null, p65-null, TNFR-null, and TRAF2-null mouse fibroblasts have been described elsewhere (Beg et al., 1995; Lin et al., 2004; Peng et al., 2007) and were maintained in DMEM complete medium with 10% FBS.

Cellular Glutathione Measurement. The intracellular levels of GSH and GSSG were determined using methods described previously (Senft et al., 2000). In brief, cells at 90% confluence were washed twice with ice-cold PBS and collected in 300 μl of homogenization buffer, containing 154 mM KCl, 5 mM diethylenetriaminepenta-acetic acid, 0.1 M KCl, and 10 mM $MgCl_2$, pH 6.8. After sonication, the homogenates were mixed with 300 μl of redox quenching buffer–trichloroacetic acid (10% trichloroacetic acid in 40 mM HCl and 10 mM diethylenetriaminepenta-acetic acid). The mixture were subjected to centrifugation at 12,000*g* for 10 min at 4°C. A fraction of the supernatant was reacted with *o*-phthalaldehyde, which bound to reduced glutathione to yield molecules with high quantum, and the GSH levels were determined spectrophotofluorometrically as described previously (Senft et al., 2000). Another fraction of the supernatant was treated by dithionite to convert GSSG to GSH and the total GSH + GSSG was determined. Molar GSH and GSSG concentrations were calculated as described elsewhere (Watson and Jones, 2003) and inserted into the Nernst equation, $\Delta E'$ $(GSSG + 2H^+ \rightarrow 2GSH) = -240\ mV - (61.5\ mV/2e^-) \cdot \log([GSH]^2/[GSSG])$, to estimate redox potentials at pH 7.0.

ROS Measurement. Direct detection of intracellular steady-state levels of ROS was carried out on living cells using 2′,7′-dichlorofluorescin-diacetate (H_2-DCFDA). Cells cultured on glass coverslips were incubated with 10 μM CM-H_2-DCFDA (Invitrogen) in FBS-free DMEM in the dark for 30 min. The cells were washed with PBS and stained with 4,6-diamidino-2-phenylindole (DAPI). ROS generation, resulting in the oxidative production of dichlorofluorescein (excitation, 488 nm; emission, 515–540 nm), was detected using fluorescence microscopy.

Alternatively, cells cultured on 10-cm^2 plates were trypsinized and resuspended in FBS-free culture medium containing 5 μM H_2-DCFDA. After incubation at 37°C for 30 min, cells were washed and suspended in PBS at 10^6 cells/ml. The cells were applied to FACSCalibur analyser (BD Immunocytometry Systems, San Jose, CA), which was equipped with a 488 Argon laser for measurements of intracellular fluorescence. Logarithmic detectors were used for the FL-1 fluorescence channel necessary for dichlorofluorescein detection. Mean log fluorescence intensity (MFI) values were obtained by the CellQuest software program (BD Biosciences).

To measure the concentration of H_2O_2, cells at approximately 10^7 cells/10-cm^2 plate were washed twice with KCl-respiratory buffer (KRB), consisting of 140 mM KCl, 2.5 mM KH_2PO_4, 2.5 mM $MgCl_2$, 1.0 mM Na_2-EDTA, 0.05% defatted recrystallized bovine serum al-

bumin, and 5 mM HEPES buffer, pH 7.4. Cells were scraped into KRB at 250 μg protein/ml. The reaction mixture for H_2O_2 release contained 100 μg of cell protein, 5 mM D(+)-glucose, 5 μM luminol (5-amino-2,3-dihydro-1,4-phthalazinedione), and 2.5 U of horseradish peroxidase/ml in a final volume of 1.0 ml of KRB. Catalase (500 U/ml) was added to half the tubes render the assay specific for H_2O_2, because catalase-inhibited luminol chemiluminescence is highly specific for H_2O_2 (Shertzer et al., 2004). Chemiluminescence was monitored at 37°C using a Berthold Autolumat Plus luminometer (Berthold Technologies, Bad Wildbad, Germany). Luminescence units in the presence of catalase were subtracted from luminescence units in the absence of catalase, and net luminescence units per microgram of protein were plotted against time. In addition, the area-under-the curve values for luminescence versus time were standardized to known H_2O_2 concentrations from 0 to 50 μM and expressed as nanomoles of H_2O_2 per milligram of protein.

Adenoviral Infection. Adenoviruses were used at a multiplicity of infection of 10 pfu/cell to infect cells at 60% confluence (Peng et al., 2007). Viral infection was carried out in serum-free DMEM for 2 h with gentle shaking. After washing with PBS, the cells were maintained in DMEM with 10% FBS for 24 h before being used in experiments.

Cell Apoptosis, Survival and Western Blot Analyses. Cell apoptosis was assessed by staining with 10 μg/ml DAPI and fluorescence microscopy observation as described previously (Peng et al., 2007). The cells with condensed or fragmented nuclei were considered to be undergoing apoptosis, and the ratio of apoptotic over total cells was thus calculated. Alternatively, apoptosis was evaluated by Annexin V-phycoerythrin Apoptosis Detection Kit (BD Pharmingen). In brief, cells were washed twice with ice-cold PBS and resuspended in 1× binding buffer at a concentration of 10^6 cells/ml. One hundred microliters of the solution (10^5 cells) were transferred to a 5-ml culture tube and incubated with 5 μl of Annexin V-phycoerythrin and 5 μl of 7-aminoactinomycin D for 15 min at room temperature in the dark. The cells were analyzed by flow cytometry. The TUNEL assay was performed using ApopTag Plus fluorescein in situ apoptosis detection kit according to manufacture's recommendation (Millipore Bioscience Research Reagents, Temecula, CA). In brief, the cells cultured on cover slips were first fixed with 1% paraformaldehyde in PBS and then fixed in precooled ethanol/acetic acid (2:1). The DNA fragments in apoptotic cells were then labeled with the digoxigenin-nucleotide, which would bind to the fluorescein conjugated anti-digoxigenin antibody applied subsequently. Finally, the cells were counterstained with DAPI and viewed by fluorescence microscopy. Micrographs of TUNEL-positive cells were taken, and the percentage of apoptosis was calculated by dividing the number of TUNEL positive cells by the number of total cells in each picture. At least 400 cells were counted for each condition.

Cell viability was determined using the tetrazolium salt 3-(4,5-dimethylthiazol-2-yl)-2,5-diphenyltetrazolium bromide (MTT), following the manufacturer's specifications (Promega, Madison, WI). Western blot analyses were done using whole-cell extracts as described previously (Peng et al., 2007).

Cell Fractionation. Cytosolic and nuclear extracts were prepared according to procedures described previously (Kann et al., 2005). For Western blot analyses, nuclear and cytosolic proteins obtained from 5×10^4 cells were boiled in SDS-polyacrylamide gel electrophoresis sample buffer and used for Western blotting analyses using anti-p65.

RNA Isolation, Fluorescent Labeling of Target cDNAs, and High-Density Microarray Hybridization and Quantitative Polymerase Chain Reaction. Total RNA was isolated from wild-type and *Ikkβ*(−/−) fibroblasts using an RNeasy kit (QIAGEN, Valencia, CA) based on the manufacturer's instructions. To verify RNA quality before labeling for microarray analyses, samples were analyzed using an Agilent 2100 Bioanalyzer (Agilent Technologies, Santa Clara, CA). For microarray work, hybridization probes were from the mouse oligonucleotide library (version 3.0; QIAGEN Operon, Alameda, CA), representing 31,769 annotated mouse genes. Hybridization targets were the paired Cy3- and Cy5-labeled control, and test cDNAs were synthesized from 20 μg of total RNA by an oligo(dT)-primed reverse transcriptase reaction and were labeled with monofunctional reactive Cy3 and Cy5 (GE Healthcare, Chalfont St. Giles, Buckinghamshire, UK). After hybridization under high-stringency conditions, slides were washed and simultaneously scanned at a 10-μm resolution at 635 (Cy5) and 532 (Cy3) nm (GenePix 4000B; Molecular Devices, Sunnyvale, CA). Comparisons were carried out with triplicate biological replicates using flipped dye arrays to allow for the removal of gene-specific dye effects. Data normalization was performed in three steps for each microarray.

For quantitative real-time PCR analyses, cDNA was synthesized by reverse transcription of 1 to 20 μg of total RNA using SuperScript II RNase H^- reverse transcriptase (Invitrogen). The cDNA was subjected to quantitative PCR using an MX3000p thermal cycler system and SYBR Green QPCR Master Mix (Stratagene, La Jolla, CA). The conditions for the PCR amplification were optimized for specific PCR reactions. At the end of the PCR, the samples were subjected to melting-curve analysis. All reactions were performed at least in triplicate. Oligonucleotides used as the specific primers to amplify mouse genes are as follows: *Gclc*, 5′-ATGACTGTTGCCAGGTGGATGAGA and 5′-ACACGCCATCCTAAACAGCGATCA; *Gclm*, 5′-AGCTGGACTCTGTGATCATGGCTT and 5′-CAAAGGCAGTCAAATCTGGTGGCA; *Gapdh*, 5′-CCATGGAGAAGGCTGGGG and 5′-CAAAGTTGTCATGGATGACC; *Ikkβ*, 5′-CTCGAACTGGTTCAAGTATCTTCGG and 5′-AACAGATCGCCATCAAGCAATGCC.

Transfection and Luciferase Reporter Assay. The *Ikkβ*(−/−) cells were grown to 60–70% confluence on a 10-cm^2 plate. The cells were transiently transfected with 10 μg of either vector control or expression vectors for *Gclc* and/or *Gclm* together with 2 μg of puromycin expression vector. At 12 h after transfection, the cells were grown in selection medium containing 1 μg/ml puromycin for 48 h and were used for experiments.

Transfection of *Ikkβ*-siRNA was performed using HiPerFect transfection reagent (QIAGEN) with fast-forward transfection protocol according to manufacture's recommendation. In brief, on the day of transfection, 5×10^6 WT MEF cells were seeded in a 10-cm^2 plate containing 6 ml of regular culture medium, followed by adding 2 ml of DMEM mixed with 0.8 nmol siRNA (giving a final siRNA concentration of 100 nM) and 200 μl of transfection reagent into the plate. The cells were incubated under normal culture condition for 48 h before further experiment.

Cells seeded in 24-well tissue culture plates at 10^5 cells/well were grown for 16 h before transfection. Transfection was carried out using Lipofectamine Plus reagent (Invitrogen), 0.5 μg of luciferase reporter, and 0.1 μg of β-galactosidase plasmids/well according to the manufacturer's instructions. Twenty-four hours after transfection, cells were deprived of serum overnight and subjected to the indicated treatments for 16 h. Cells were lysed, and luciferase activity and β-galactosidase activity were determined using the luciferase reporter and β-galactosidase reporter kits (Promega).

Chromatin Immunoprecipitation Analyses. Chromatin immunoprecipitation (ChIP) was performed using wild-type and *Ikkβ*(−/−) cells using methods described previously (Schnekenburger et al., 2007). In brief, cells were treated with formaldehyde, and chromatin was prepared and sheared to a size range of 0.3 to 0.6 kbp by sonication in a crushed-ice/water bath with six 30-s bursts of 200 W, with a 30-s interval between bursts using a Bioruptor (Diagenode). Chromatin was immunoprecipitated overnight using antibodies for c-JUN, NFκB p50/p65, and nonspecific rabbit IgG. The immune complexes were allowed to react with protein A-agarose beads (Millipore); after extensive washing, the precipitates were removed from the beads using elution buffer (50 mM $NaHCO_3$ and 1% SDS) and mild vortexing. The cross-linking was reversed and the samples were sequentially digested with RNase A and proteinase K. Precipitated DNA was purified by chromatography on QIAquick columns (QIAGEN) and subjected to real-time PCR. For a complete

coverage of the region between −2.0 kbp and +1 base pair of the mouse *Gclc* and −1.5 and +0.5 kbp of the mouse *Gclm* promoters, five primer sets were designed for each gene and tested in PCR reactions with genomic DNA as the template. For the purpose of size confirmation, endpoint PCR products were separated by electrophoresis through 15% polyacrylamide gels and visualized after staining with ethidium bromide. Relative cycle differences in QRT-PCR were determined using ΔC_T determined by the cycle threshold (C_T) value of ChIP DNA normalized to the C_T of input DNA. QPCR results are shown as fold change in specific antibody immunoprecipitation over IgG nonspecific immunoprecipitation controls.

Statistical Analysis. Statistical analyses of microarray data were performed by fitting the mixed-effects linear model for each gene separately, as discussed in detail previously (Kann et al., 2005). Resulting *t* statistics from each comparison were then adjusted using a hierarchical empirical Bayes model (Smyth, 2004) for calculation of *P* values and using the expected number of false positives based on the false discovery rate (Klipper-Aurbach et al., 1995). For other statistical analyses, comparisons were performed using Student's two-tailed paired *t* test or multiple comparison ANOVA.

Results

Genetic and Pharmacological Inactivation of the Canonical IKKβ Pathway Causes GSH Deficiency. We have shown previously that fibroblasts deficient in IKKβ have a high level of ROS accumulation in response to arsenic and are extremely sensitive to arsenic toxicity (Peng et al., 2007). In this regard, *Ikkβ*(−/−) cells are similar to cells deficient in glutathione, which also have a high prooxidant status (Kann et al., 2005). To test whether the susceptibility of IKKβ-null cells to oxidative stress induced by arsenic was also related to glutathione deficiency, we measured intracellular GSH and GSSG levels and calculated the corresponding redox coupling potentials. Reduced GSH levels were high at 31 nmol/mg protein in wild-type cells and were nearly 5-fold lower in *Ikkβ*(−/−) cells (Fig. 1A). The redox potential of the GSSG/2GSH couple was calculated (Watson and Jones, 2003) to be −176 mV in wild-type cells and was decreased to half that level in *Ikkβ*(−/−) cells. Expression of IKKβ, but not β-galactosidase, in the *Ikkβ*(−/−) cells significantly elevated GSH contents and reducing potential of the redox couple (Fig. 1A), indicating that the effects seen in the *Ikkβ*(−/−) were due primarily to the lack of IKKβ and not to compensatory mechanisms established during embryonic development.

In the classic NF-κB pathway, IKKβ is responsible for transmitting signals from upstream TNFR1 and TRAF2/5 to downstream p65/RelA. To test whether other components of this pathway were also involved in modulating redox potential, we measured GSH and GSSG values in cells deficient in TNFR1, TRAF2, and p65 (Fig. 1A). Both TNFR1 and p65 are essential for pathway activation; likewise, the *Tnfr1*(−/−) and *p65*(−/−) cells had nearly 80% reduction of GSH compared with the wild-type cells. TRAF2, on the other hand, is not essential for classic pathway activation, and the *Traf2*(−/−) had only 50% GSH reduction. Likewise, the reducing potential was decreased significantly in *Tnfr1*(−/−) and *p65*(−/−) cells and less so in *Traf2*(−/−) cells. Based on these studies, we suggest that the classic IKK pathway is required for maintaining the homeostatic levels of GSH in mouse fibroblasts.

Although the physiologic role of the IKKβ pathway has mostly been studied using genetic inactivation of IKKβ in mice, *IKKβ* gene mutations have not been found in homozygosity linked to human diseases. In clinical settings, pharmaceutical inhibition of IKKβ signaling is commonly used for anti-inflammation and pain alleviation purposes, posing the question of whether IKKβ or NF-κB inhibition by chemicals may achieve effects similar to those of genetic IKKβ ablation. We chose three commercially available inhibitors (JSH23, a cell-permeant diamino compound that blocks p65/RelA nuclear translocation and activation, and BMS-345541 and TPCA-1, potent and specific inhibitors of IKKβ) to evaluate the consequence of IKKβ and NF-κB inhibition. Treatment of wild-type fibroblasts with these inhibitors caused reduced GSH content and lower redox potential (Fig. 1B). Thus, genetic and pharmaceutical inactivation of the NF-κB pathway are similar, in the sense that they both cause inhibition of

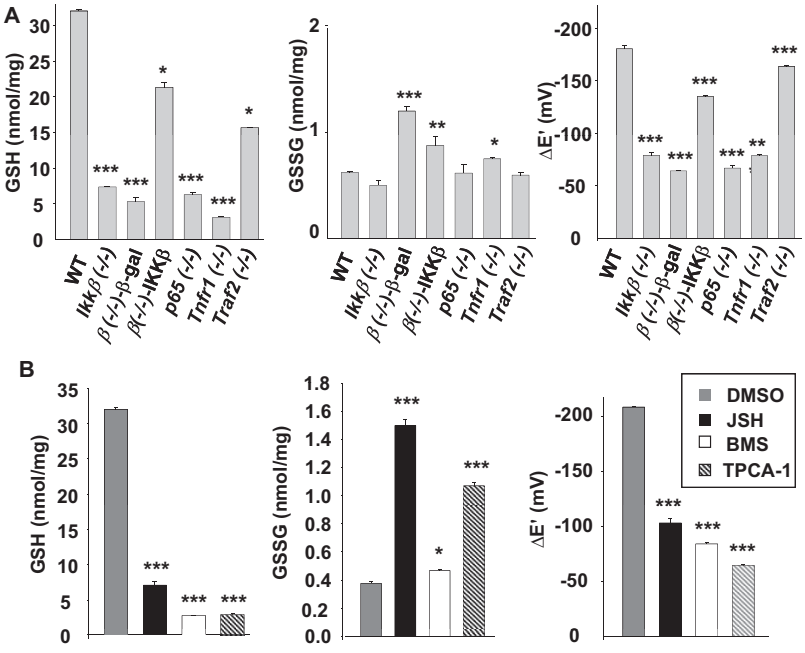

Fig. 1. Genetic and pharmacological IKKβ pathway inactivation causes GSH deficiency. A, wild-type, knockout and *Ikkβ*(−/−) cells infected with Ad β-gal [β(−/−)-β-gal] or Ad IKKβ [β(−/−)-IKKβ]. B, wild-type fibroblasts treated for 24 h with 0.1% DMSO, 10 μM JSH23, 1 μM BMS-345541, and 0.5 μM TPCA-1, as indicated, were collected, and cell lysates were used for measurement of GSH and GSSG contents and calculation of GSH/GSSH redox potentials. All results are presented as the mean values ± S.E. from at least three independent experiments. Statistical analyses were done compared with the mean values in control wild-type cells and **, $p < 0.01$; ***, $p < 0.001$ were considered significant.

basal NF-κB activity and decrease in intracellular GSH and redox potential.

Loss of IKKβ Signaling Sensitizes Cells to the Cytotoxicity of Pharmacological and Environmental Agents. GSH is one of the most important antioxidants, which protect the organism against a broad range of physiological and environmental stresses (Meister and Anderson, 1983; Townsend et al., 2003). We sought to determine whether IKKβ-deficient cells, with reduced GSH levels, were more vulnerable to stress toxicity. We treated wild-type and IKKβ-deficient cells with various stress stimuli and evaluated cell survival. The treatments include the oxidative stress inducer H_2O_2, the DNA-damaging agents etoposide and cisplatin, and the microtubule toxins paclitaxel (Taxol) and colchicine, (Varbiro et al., 2001; Kurosu et al., 2003; Taniguchi et al., 2005; Alexandre et al., 2006). Relative to wild-type cells, *Tnfr1*(−/−) and *Ikkβ*(−/−) cells and, to a lesser extent, *Traf2*(−/−) cells, showed decreased survival in response to all five stress stimuli (Fig. 2A). Arsenic is an environmental toxic agent that can modify mitochondrial respiration, leading to ROS production and cell apoptosis (Ralph, 2008). We found that genetic knockout (Fig. 2A) and knock-down (Fig. 2, B and C) of *Ikkβ* and pharmacological inactivation (Fig. 2D) of IKKβ signaling significantly enhanced arsenic toxicity. These findings strongly suggest that IKKβ signaling is required for protecting cells against oxidative stress elicited by pharmacological and environmental agents.

Reduced GCLC and GCLM Expression in *Ikkβ*(−/−) Cells. Using DCFDA, we detected a slightly elevated ROS in the *Tnfr1*(−/−), *Traf2*(−/−), and *Ikkβ*(−/−) cells compared with the wild-type cells (Fig. 3A). Likewise, using luminol chemiluminescence, we found that the H_2O_2 levels were slightly elevated in *Traf2*(−/−) but significantly increased in *Tnfr1*(−/−) and *Ikkβ*(−/−) compared with wild-type cells (Fig. 3B). The higher ROS in the knockout cells, however, was insufficient to cause a significant change in GSH oxidation, because the levels of GSSG were the same in wild-type and IKKβ-deficient cells (Fig. 1A). Thus, we suggest that GSH deficiency in the IKKβ deficient cells was not due to increased oxidative GSH depletion.

Alternatively, GSH deficiency in IKKβ-deficient cells could be due to increase in GSH exportation. To determine whether this was the case, we measured extracellular GSH content in the growth media. The extracellular GSH was low overall, but it corresponded well with the intracellular levels in the different cells tested. Thus, the wild-type and Ad-IKKβ-infected *Ikkβ*(−/−) cells had slightly higher levels of extracellular GSH than the IKKβ-deficient cells (Supplemental Fig. S1). ATP-binding cassette transporters mediate GSH exportation to the extracellular milieu. In a genome-wide expression profiling experiment, we found no apparent differences in the levels of Abcc1, Abcc2, Abcc3, Abcc4, Abcc5, Abcc6, Abcc8, Abcc9, Abcc10, or Abcc12 mRNA in wild-type and *Ikkβ*(−/−) cells (data not shown). Together, these observations suggest that IKKβ signaling helps to maintain cellular GSH through mechanisms independent of GSH consumption or export.

Glutathione homeostasis depends critically on a set of glutathione redox cycling enzymes. GCL and GSH synthase are responsible for biosynthesis and GSR for reduction of GSSG to GSH. On the other hand, GPX and CYP2E1 catalyze GSH to generate oxidized GSSG. In genome-wide expression studies, we found that IKKβ ablation caused a significant reduction in Gclc and Gclm mRNA, although it had less effect on the levels of other GSH redox cycling enzymes (Table 1). Using real-time RT-PCR, we further confirmed that the *Ikkβ*(−/−) cells had 58% reduction of Gclc and 67% reduction of Gclm mRNA compared with wild-type cells (Fig. 3C). Likewise, the *Ikkβ*(−/−) cells had reduced GCLC and GCLM proteins. Reconstitution of IKKβ expression in the *Ikkβ*(−/−) cells markedly elevated the GCLC and GCLM proteins (Fig. 3D); on the other hand, treatment of wild-type cells with IKKβ signaling inhibitors markedly reduced the levels of both Gclc and Gclm (Fig. 3E). These observations

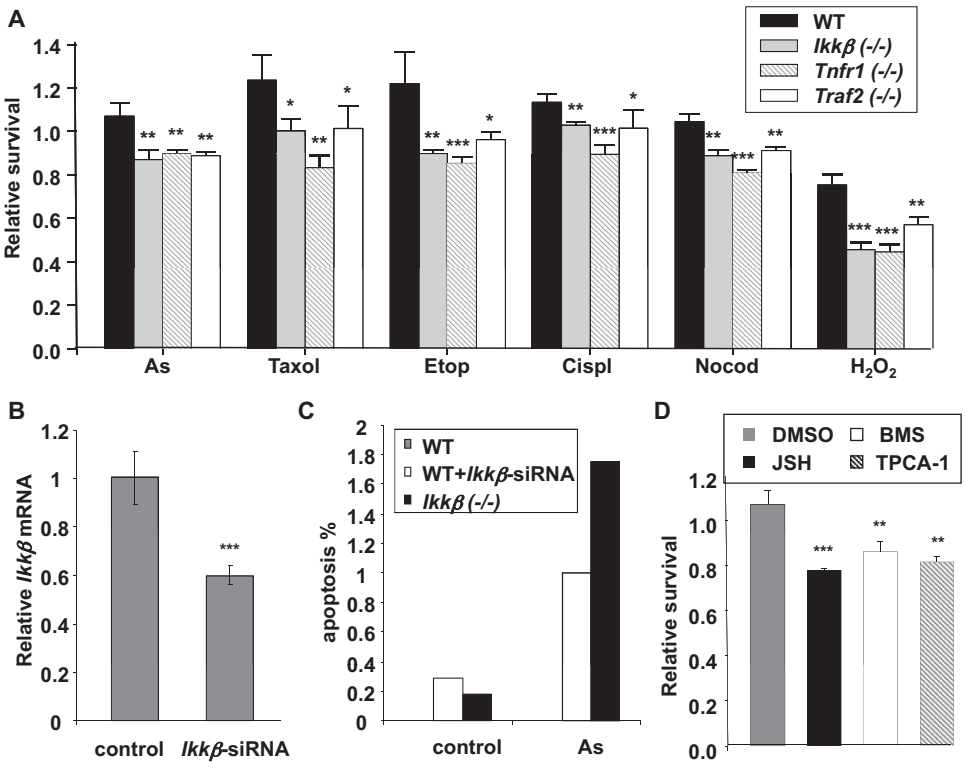

Fig. 2. IKKβ and NF-κB inactivation reduces cell survival in response to oxidative damage. A, wild-type and gene-knockout fibroblasts were treated for 24 h with various oxidative agents, including 10 μM sodium arsenite (As), 50 μM hydrogen peroxide (H_2O_2), 50 μM cisplatin (Cispl), 50 μM etoposide (Etop), 5 μM paclitaxel (Taxol), and 5 μM nocodazole (Nocod). Cell viability was measured by MTT assay. B, wild-type fibroblasts were transfected with either scrambled or *Ikkβ*-siRNA (100 nM). The relative *Ikkβ* expression was determined by real-time RT-PCR. The *Ikkβ* levels in scrambled RNA transfected cells are designated as 1. C, the wild-type cells with or without *Ikkβ*-siRNA transfection and Ikkβ(−/−) cells were treated with 50 μM arsenic for 2 h. Apoptosis was measured by TUNEL assay. The values represent the average of at least 400 cells counted. D, wild-type fibroblasts treated for 2 h with 0.1% DMSO, 10 μM JSH23, 1 μM BMS-345541, and 0.5 μM TPCA-1, followed by treatment with 10 μM sodium arsenite for 24 h. Cell viability was measured by MTT assay. All results are presented as the mean values ± S.E. from at least three independent experiments. Statistical analyses were done compared with the mean values in control wild-type cells and **, $p < 0.01$; ***, $p < 0.001$ were considered significant.

support a role for IKKβ signaling in optimal GCLC and GCLM expression and activities (Fig. 3F).

IKKβ-Dependent NF-κB Binding and Activation of the *Gcl* Promoters. To address whether the IKKβ pathway was required for transcriptional activation of the *Gclc* and *Gclm* promoters, we measured *Gclc*- and *Gclm*-promoter driven luciferase activities in wild-type and knockout cells (Fig. 4A). Compared with wild-type cells, *Gclc*-luciferase activity was decreased slightly in *Traf2*(−/−) cells but reduced markedly in *Ikkβ*(−/−) cells and more so in *Tnfr1*(−/−) cells. Likewise, *Gclm*-luciferase activity was reduced by 60 to 80% in *Tnfr1*(−/−), *Ikkβ*(−/−), and *Traf2*(−/−) cells compared with wild-type cells.

The transcription factors NF-κB, AP-1, and NRF2 mediate *Gclc* and *Gclm* gene induction (Yang et al., 2005a,b). To identify which of these factors might act downstream of the IKKβ signaling in the regulation of the *Gcl* promoters, we measured the activity of each transcription factor in wild-type and knockout cells using luciferase reporter systems. We found that the basal NF-κB activity was highest in wild-type and IKKβ-reconstituted *Ikkβ*(−/−) cells, slightly lower in *Traf2*(−/−) cells, but much reduced in *Ikkβ*(−/−) and *Tnfr1*(−/−) cells (Fig. 4B). Examination of nuclear localization of active RelA/p65 led to the same conclusion. Approximately 10% of the total RelA/p65 was found in the nucleus of wild-type cells and 1% in the nucleus of *Traf2*(−/−) cells, whereas there was no detectable nuclear RelA/p65 in *Ikkβ*(−/−) or *Tnfr1*(−/−) cells (Fig. 4C). TNFα further potentiated NF-κB activity and nuclear translocation in wild-type and *Traf2*(−/−), but it caused very little, if any, NF-κB activation in *Tnfr1*(−/−) and *Ikkβ*(−/−) cells (Fig. 4C and Supplemental Fig. S2). Treatment of the wild-type cells with IKKβ signaling inhibitors prevented basal and TNFα induced p65/RelA nuclear translocation and significantly reduced NF-κB activity, similar to the effects of genetic IKKβ pathway inactivation (Fig. 4, C and D). It is noteworthy that there was a good correlation between basal activities of NF-κB and *Gcl* promoters in all the experimental conditions examined. In contrast, we found that the basal NRF2 and AP-1 activities were not reduced but instead increased in *Ikkβ*(−/−) and *p65*(−/−) cells relative to wild-type or IKKβ-reconstituted *Ikkβ*(−/−) cells, making it unlikely that these factors were involved in IKKβ-dependent *Gcl* promoter activation (Fig. 4E).

Potential binding sites for NF-κB were found using CHIP-MAPPER throughout the 2-kb regions in the mouse *Gclc* and *Gclm* promoters. To assess whether NF-κB directly interacts with the *Gclc* and *Gclm* promoters, we performed ChIP assays (Fig. 5). The ChIP results showed that p65/p50 NF-κB interacts with regions in both distal and proximal *Gclc* and *Gclm* promoters with higher efficiency in wild-type than in *Ikkβ*(−/−) cells. In contrast, c-Jun interacts with a distal region of the *Gclc* promoter with higher efficiency in *Ikkβ*(−/−) cells, consistent with higher c-Jun activities in these cells. In the unstressed fibroblasts, we did not detect direct c-Jun interactions with the mouse *Gclm* promoter. These observations argue against a positive regulatory role of c-Jun in *Gclc* and *Gclm* promoter activation in unstressed conditions but, on the other hand, suggest that a more abundant NF-κB occupancy of the *Gclc* and *Gclm* promoters might be responsible for higher promoter activation in wild-type cells.

Increased GCLC and GCLM Expression Elevates GSH in *Ikkβ*(−/−) Cells. To test whether the reduced GCLC and GCLM expression was responsible for GSH deficiency in the *Ikkβ*(−/−) cells, we introduced transiently ei-

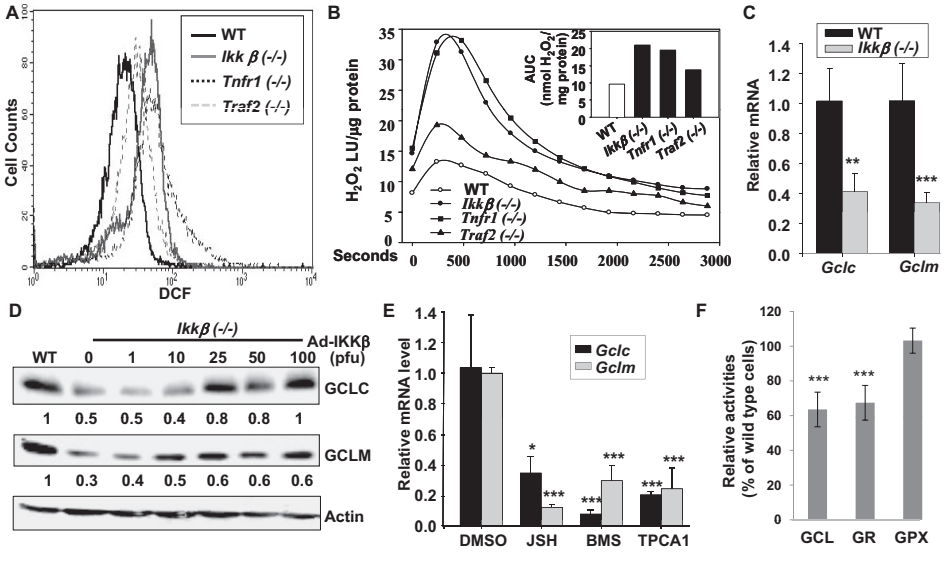

Fig. 3. Inactivation of the IKKβ pathway reduces GCLC and GCLM expression. Wild-type, *Ikkβ*(−/−), *Tnfr1*(−/−), and *Traf2*(−/−) cells were labeled with CM-H2DCFDA under normal growth conditions and were analyzed by Flow cytometry (A), and used for measurement of H_2O_2 release by catalase-inhibited luminol chemiluminescence (B). The time-courses for H_2O_2 release are shown in the line plots as luminescence units (LU)/μg cell protein, with the insert depicting the area under each curve (AUC) as nanomoles of H_2O_2 release per milligram of protein. Each value represents the average of two experiments. Total RNA was isolated from wild-type and *Ikkβ*(−/−) cells (C), and wild-type cells were treated for 24 h with 0.1% DMSO, 10 μM JSH23, 1 μM BMS-345541, and 0.5 μM TPCA-1 (E). The RNA were subjected to reverse transcription followed by quantitative RT-PCR. Results showed the levels of *Gclc*/*Gapdh* and *Gclm*/*Gapdh* in *Ikkβ*(−/−) relative to those in wild-type cells designated as 1. D, total cell lysates from wild-type, *Ikkβ*(−/−), and *Ikkβ*(−/−) cells infected with IKKβ adenovirus were subjected to Western blotting. The GCLC/β-actin and GCLM/β-actin levels were compared with those in wild-type cells designated as 1. F, enzyme activities in *Ikkβ*(−/−) cells were compared with those in wild-type cells, designated as 100%. All results are presented as the mean values ± S.E. from at least three independent experiments. Statistical analyses were done compared with the mean values in control wild-type cells. **, $p < 0.01$; ***, $p < 0.001$ were considered significant.

ther empty, GCLC, or GCLM expression vectors into *Ikkβ*(−/−) cells and measured GSH and GSSG. The GSH levels were significantly elevated in GCLC- and GCLM-overexpressing *Ikkβ*(−/−) cells with levels 2- to 3-fold higher than those in cells transfected with the empty vector (Fig. 6A). Likewise, the reducing potential in the *Ikkβ*(−/−) cells was increased from $\Delta E'$ −49 to −165 mV with GCLC ectopic expression and to −127 mV with GCLM ectopic expression.

Exogenous GCLC and GCLM expression in the *Ikkβ*(−/−) cells also effectively prevented the induction of ROS by arsenic, as DCFDA-positive *Ikkβ*(−/−) cells were easily detectable in control, vector-transfected cells but not in *Gclc*/*Gclm* transfected cells (Fig. 6B). Concurrently, the *Gclc*/*Gclm*-transfected *Ikkβ*(−/−) cells were protected from arsenic-induced apoptosis (Fig. 6, C and D). Hence, IKKβ-mediated optimal GCLC and GCLM expression helps to maintain cellular GSH levels and electronegative $\Delta E'$ values, which in turn is required for protecting cells against oxidative stress toxicity.

TABLE 1
Gene expression of redox cycling enzymes

Gene Name	Symbol	Avg Int	WT:IKKβ(−/−)
GSH biosynthesis			
Glutamate-cysteine ligase, modifier	*Gclm*	1726	2.53
Glutamate-cysteine ligase, catalytic	*Gclc*	481	1.52
Glutathione synthetase	*Gss*	287	1.47
GSH redox cycling enzymes			
Glutathione reductase 1	*Gsr*	793	1.41
Glutathione peroxidase 1	*Gpx1*	3462	−1.03
Glutathione peroxidase 2	*Gpx2*	39	1.10
Glutathione peroxidase 3	*Gpx3*	61	1.06
Glutathione peroxidase 4	*Gpx4*	7635	1.03
Glutathione peroxidase 5	*Gpx5*	24	1.12
Glutathione peroxidase 6	*Gpx6*	28	1.19
Glutathione peroxidase 7	*Gpx7*	39	−1.13
Cytochrome p450, 2e1	*Cyp2ef*	23	1.12

WT, wild type.

Discussion

The classic IKKβ-NF-κB pathway has a fundamental role in modulating innate and adaptive immune responses. In this context, activation of this pathway leads to immediate induction of pro-inflammatory cytokines, such as TNFα, that, in addition to their antipathogenic effect, can further activate the IKKβ-NF-κB pathway, thereby propagating and amplifying the inflammatory responses. Recent genetic and chemical inhibitor studies have uncovered new functions of this pathway that may not be directly linked to inflammation (Hayden and Ghosh, 2008). Here we show that basal low-level activation of the IKKβ-NF-κB pathway plays a pivotal role in maintaining GSH homeostasis. Genetic and pharmacological inactivation of this pathway results in severe glutathione deficiency that leads to increased sensitivity to toxicity caused by a broad range of environmental and therapeutic agents.

Both basal and TNFα-induced NF-κB activities are greatly reduced in *Traf2*(−/−) and almost completely abolished in *Tnfr1*(−/−) and *Ikkβ*(−/−) cells. This observation supports the idea that the TNFα-induced classic IKKβ cascade is normally maintained at a low constitutively active state, leading to slow IκBα degradation and steady state NF-κB activation, whereas excessive exogenous TNFα accelerates and amplifies this reaction, causing more abundant NF-κB activation (O'Dea et al., 2008). Although robust activation of the IKKβ-NF-κB pathway is known to activate proinflamma-

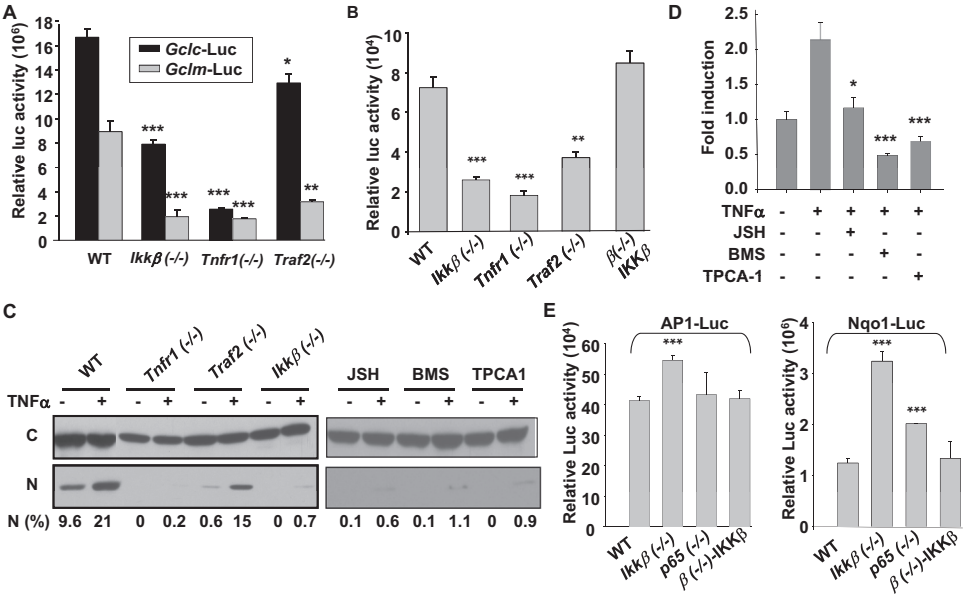

Fig. 4. Inactivation of the IKKβ pathway affects transcription factor activities. A, wild-type, *Ikkβ*(−/−), *Tnfr1*(−/−), and *Traf2*(−/−) cells were transfected with β-gal expression plasmids together with *Gclc*-Luc and *Gclm*-Luc. The relative luciferase activities were normalized to β-galactosidase activities measured 24 h after transfection. Wild-type, various knockout cells, and *Ikkβ*(−/−) cells infected with Ad IKKβ [β(−/−)-IKKβ] were transiently transfected with β-gal expression plasmids, together with and AP-1-luc (B) and Nqo1-luc (E). D, wild-type cells were transfected with NF-κB-luc and β-gal plasmids for 24 h, followed by inhibitor and TNFα treatment for 16 h. The relative luciferase activities were normalized to β-galactosidase activities measured 24 h after transfection. All results are presented as the mean values ± S.E. from at least three independent experiments. Statistical analyses were done compared with the mean values in control wild-type cells and **, $p < 0.01$; ***, $p < 0.001$ were considered significant. C, cells were either untreated or treated with TNFα (10 ng/ml) for 0.5 h. Cytoplasmic and nuclear extracts from 500,000 cells were analyzed by Western blotting using anti-p65 and the relative levels of nuclear p65 [*N* (%)] were calculated after densitometric quantification of chemiluminescence.

tory transcriptional programs, the basal NF-κB activity may dictate different transcription trajectories. We show that IKKβ ablation affects the expression of genes involved in GSH homeostasis, important for maintenance of biological systems (Chen et al., 2003; Peng et al., 2007). Because NF-κB is known to be activated by low levels of ROS and inhibited by antioxidants (Mantena and Katiyar, 2006), maintaining GSH homeostasis may serve as an autocrine regulatory mechanism through which the IKKβ-NF-κB pathway provides feedback to keep its own activity in check.

The NF-κB is required for optimal expression of antioxidants, including the cytochrome P450 CYP1B1, MnSOD, FHL, and metallothionein (Chen et al., 2003; Pham et al., 2004; Kamata et al., 2005; Peng et al., 2007); however, none of these known NF-κB targets has a major role in GSH homeostasis. We find that the IKKβ-dependent NF-κB transcription factor directly interacts with the *Gclc* and *Gclm* promoters and that the extent of the binding correlates with the level of GCLC/GCLM expression and GSH content. Induction of the *Gclc* and *Gclm* promoters under oxidative stress conditions is mediated by redox-sensitive transcription factors (Jeyapaul and Jaiswal, 2000; Yang et al., 2001; Na-

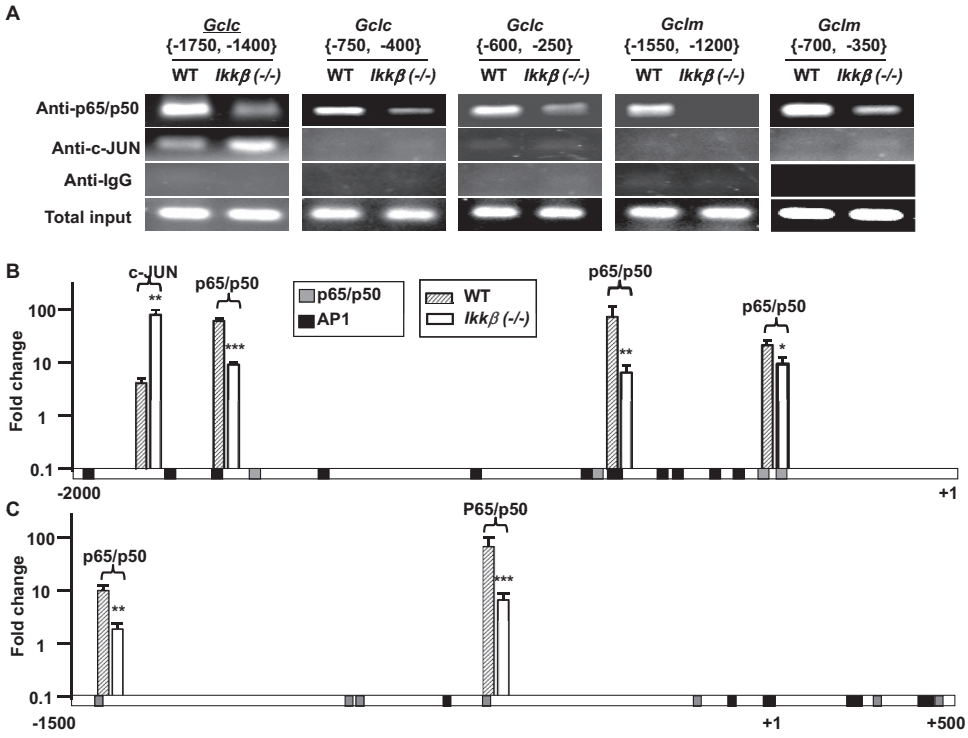

Fig. 5. Regulation of GCLC/GCLM expression by the IKKβ pathway. A, Antibodies against p65 and p50, c-Jun, and control IgG were used for ChIP using chromatin isolated from unstressed wild-type and *Ikk*β(−/−) cells. The precipitates were subjected to PCR amplification using primers for various regions of the *Gclc* and *Gclm* promoters, as indicated in brackets. The PCR-amplified genomic DNA without ChIP was used as total input control. The PCR products were resolved on a gel and photographed. CHIP-MAPPER analyses showed potential NF-κB (p50/p65) (green) and AP-1 (orange) binding sites in the −2000 to +1 base pair promoter of *Gclc* (B) and the −1500 to + 500 promoter of *Gclm* (C). The ChIP data represent fold change over IgG control determined by $2^{-\Delta\Delta C_T}$ resulting from qRT-PCR (see Supplemental Materials). Statistical analyses were done by comparing the mean values in wild-type (black bars) and *Ikk*β(−/−) (gray bars) cells.

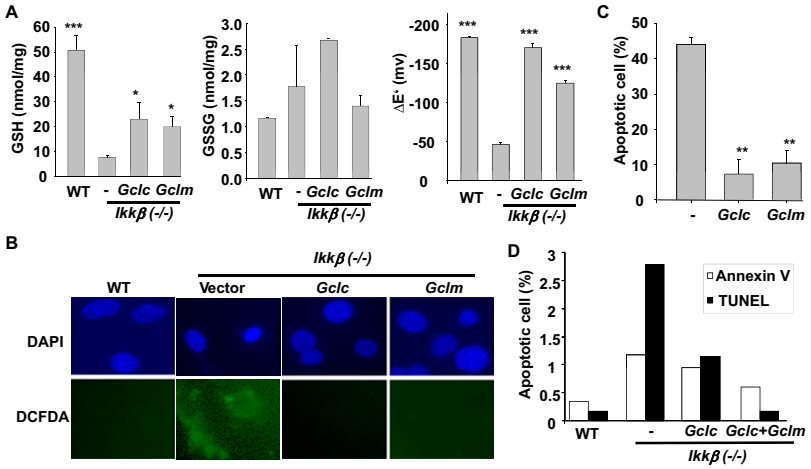

Fig. 6. Overexpression of GCLC and GCLM in *Ikk*β(−/−) cells partially restores GSH levels. Wild-type and *Ikk*β(−/−) cells were transfected with empty or GCLC and GCLM expression vectors for 24 h. A, GSH and GSSG levels were measured and redox potentials calculated as in Fig. 1. B, cells were treated with sodium arsenite (50 μM) for 6 h, followed by CM-H_2DCFDA labeling. The nuclei were identified after staining with DAPI (blue) and the ROS-activated dichlorofluorescein fluorescence (green) was observed with fluorescence microscopy. Wild-type and/or the *Ikk*β(−/−) cells transfected with empty or GCLC and GCLM expression vectors were treated with 50 μM sodium arsenite for 6 h. C, the cells were stained with DAPI, and cells with condensed nuclei (i.e., apoptotic cells) were identified under fluorescence microscopy. Numbers represent three fields of triplicate samples. Results were the mean values ± S.E. from at least three independent experiments. Statistical analyses were done by comparing the mean values in untransfected *Ikk*β(−/−) cells. *, $p < 0.05$; **, $p < 0.01$; ***, $p < 0.001$ are considered significant. D, the cells were subjected to Annexin V staining and TUNEL analyses. The number of Annexin V and TUNEL-positive cells was counted, and the percentage of apoptosis was calculated based on total cell number.

gashima et al., 2007; Lu, 2009). Specifically, stress-activated NRF2 up-regulates AP-1 and NF-κB, which in turn bind to and activate the *Gclc* and *Gclm* promoters (Urata et al., 1996; Yang et al., 2005a,b). We find that the IKKβ-null cells have slightly higher AP-1 and NRF2 activities probably due to elevated ROS (Fig. 3A), but they have lower NF-κB activity, corresponding to lower *Gcl* promoter activation. Thus, maintenance of basal *Gcl* promoter activity under normal non-stress condition seems to depend on IKKβ-mediated NF-κB but not on c-Jun- or NRF2-mediated NF-κB induction. These observations further suggest that the transcriptional machinery involved in maintaining the basal activity of the *Gcl* promoters is different from that activated by physiological and environmental stresses.

GSH is an abundant thiol-containing small molecule that plays an evolutionarily conserved role in maintaining an intracellular reducing environment (Meister and Anderson, 1983). Low levels of GCLC/GCLM expression in cells deficient in IKKβ may lead to GSH deficiency and ultimately may be responsible for a wide variety of diseases resulting from excess oxidative stress, including cancer, neurodegenerative disorders and aging (Townsend et al., 2003). In this regard, GSH deficiency resulting from inactivation of the IKKβ-NF-κB pathway may be responsible for some of the physiological and pathological phenomena observed in *Ikkβ*(−/−) mice, such as those occurring in chemically induced liver carcinogenesis and increased insulin sensitivity. Hence, pharmacological inhibition of the IKKβ-NF-κB pathway may not only suppress inflammatory responses, but also cause GSH deficiency, leading to broader and long-term physiopathological consequences.

Acknowledgments

We thank Drs. Michael Karin for *Ikkβ*(−/−) MEFs; Ebrahim Zandi for *Ikkβ*(−/−)-R cells; Sankar Ghosh for *p65*(−/−); Yinling Hu for IKKβ adenovirus; Tim Dalton, Daniel Nebert, and Ying Chen for the *Gclc*/*Gclm* expression vectors and the GCLC/M antibodies; and Dr. Shelly C. Lu for *Gclc*-Luc/*Gclm*-Luc plasmids.

References

Alexandre J, Batteux F, Nicco C, Chéreau C, Laurent A, Guillevin L, Weill B, and Goldwasser F (2006) Accumulation of hydrogen peroxide is an early and crucial step for paclitaxel-induced cancer cell death both in vitro and in vivo. *Int J Cancer* **119:**41–48.

Beg AA, Sha WC, Bronson RT, Ghosh S, and Baltimore D (1995) Embryonic lethality and liver degeneration in mice lacking the RelA component of NF-kappa B. *Nature* **376:**167–170.

Boitier E, Merad-Boudia M, Guguen-Guillouzo C, Defer N, Ceballos-Picot I, Leroux JP, and Marsac C (1995) Impairment of the mitochondrial respiratory chain activity in diethylnitrosamine-induced rat hepatomas: possible involvement of oxygen free radicals. *Cancer Res* **55:**3028–3035.

Chen F, Castranova V, Li Z, Karin M, and Shi X (2003) Inhibitor of nuclear factor kappaB kinase deficiency enhances oxidative stress and prolongs c-Jun NH_2-terminal kinase activation induced by arsenic. *Cancer Res* **63:**7689–7693.

Cosulich SC, James NH, Needham MR, Newham PP, Bundell KR, and Roberts RA (2000) A dominant negative form of IKK2 prevents suppression of apoptosis by the peroxisome proliferator nafenopin. *Carcinogenesis* **21:**1757–1760.

Hayden MS and Ghosh S (2008) Shared principles in NF-kappaB signaling. *Cell* **132:**344–362.

Hoffer A, Chang CY, and Puga A (1996) Dioxin induces transcription of fos and jun genes by Ah receptor-dependent and -independent pathways. *Toxicol Appl Pharmacol* **141:**238–247.

Jeyapaul J and Jaiswal AK (2000) Nrf2 and c-Jun regulation of antioxidant response element (ARE)-mediated expression and induction of gamma-glutamylcysteine synthetase heavy subunit gene. *Biochem Pharmacol* **59:**1433–1439.

Kamata H, Honda S, Maeda S, Chang L, Hirata H, and Karin M (2005) Reactive oxygen species promote TNFalpha-induced death and sustained JNK activation by inhibiting MAP kinase phosphatases. *Cell* **120:**649–661.

Kann S, Estes C, Reichard JF, Huang MY, Sartor MA, Schwemberger S, Chen Y, Dalton TP, Shertzer HG, Xia Y, et al. (2005) Butylhydroquinone protects cells genetically deficient in glutathione biosynthesis from arsenite-induced apoptosis without significantly changing their prooxidant status. *Toxicol Sci* **87:**365–384.

Klipper-Aurbach Y, Wasserman M, Braunspiegel-Weintrob N, Borstein D, Peleg S, Assa S, Karp M, Benjamini Y, Hochberg Y, and Laron Z (1995) Mathematical formulae for the prediction of the residual beta cell function during the first two years of disease in children and adolescents with insulin-dependent diabetes mellitus. *Med Hypotheses* **45:**486–490.

Kurosu T, Fukuda T, Miki T, and Miura O (2003) BCL6 overexpression prevents increase in reactive oxygen species and inhibits apoptosis induced by chemotherapeutic reagents in B-cell lymphoma cells. *Oncogene* **22:**4459–4468.

Lin Y, Choksi S, Shen HM, Yang QF, Hur GM, Kim YS, Tran JH, Nedospasov SA, and Liu ZG (2004) Tumor necrosis factor-induced nonapoptotic cell death requires receptor-interacting protein-mediated cellular reactive oxygen species accumulation. *J Biol Chem* **279:**10822–10828.

Lu SC (2009) Regulation of glutathione synthesis. *Mol Aspects Med* **30:**42–59.

Maeda S, Kamata H, Luo JL, Leffert H, and Karin M (2005) IKKbeta couples hepatocyte death to cytokine-driven compensatory proliferation that promotes chemical hepatocarcinogenesis. *Cell* **121:**977–990.

Mantena SK and Katiyar SK (2006) Grape seed proanthocyanidins inhibit UV-radiation-induced oxidative stress and activation of MAPK and NF-kappaB signaling in human epidermal keratinocytes. *Free Radic Biol Med* **40:**1603–1614.

Meister A and Anderson ME (1983) Glutathione. *Annu Rev Biochem* **52:**711–760.

Nagashima R, Sugiyama C, Yoneyama M, Kuramoto N, Kawada K, and Ogita K (2007) Acoustic overstimulation facilitates the expression of glutamate-cysteine ligase catalytic subunit probably through enhanced DNA binding of activator protein-1 and/or NF-kappaB in the murine cochlea. *Neurochem Int* **51:**209–215.

O'Dea EL, Kearns JD, and Hoffmann A (2008) UV as an amplifier rather than inducer of NF-kappaB activity. *Mol Cell* **30:**632–641.

Pahl HL (1999) Activators and target genes of Rel/NF-kappaB transcription factors. *Oncogene* **18:**6853–6866.

Peng Z, Peng L, Fan Y, Zandi E, Shertzer HG, and Xia Y (2007) A critical role for IkappaB kinase beta in metallothionein-1 expression and protection against arsenic toxicity. *J Biol Chem* **282:**21487–21496.

Pham CG, Bubici C, Zazzeroni F, Papa S, Jones J, Alvarez K, Jayawardena S, De Smaele E, Cong R, Beaumont C, et al. (2004) Ferritin heavy chain upregulation by NF-kappaB inhibits TNFalpha-induced apoptosis by suppressing reactive oxygen species. *Cell* **119:**529–542.

Ralph SJ (2008) Arsenic-based antineoplastic drugs and their mechanisms of action. *Met Based Drugs* **2008:**260146.

Sakon S, Xue X, Takekawa M, Sasazuki T, Okazaki T, Kojima Y, Piao JH, Yagita H, Okumura K, Doi T, et al. (2003) NF-kappaB inhibits TNF-induced accumulation of ROS that mediate prolonged MAPK activation and necrotic cell death. *EMBO J* **22:**3898–3909.

Schnekenburger M, Talaska G, and Puga A (2007) Chromium cross-links histone deacetylase 1-DNA methyltransferase 1 complexes to chromatin, inhibiting histone-remodeling marks critical for transcriptional activation. *Mol Cell Biol* **27:**7089–7101.

Senft AP, Dalton TP, and Shertzer HG (2000) Determining glutathione and glutathione disulfide using the fluorescence probe *o*-phthalaldehyde. *Anal Biochem* **280:**80–86.

Shertzer HG, Clay CD, Genter MB, Chames MC, Schneider SN, Oakley GG, Nebert DW, and Dalton TP (2004) Uncoupling-mediated generation of reactive oxygen by halogenated aromatic hydrocarbons in mouse liver microsomes. *Free Radic Biol Med* **36:**618–631.

Sierra-Rivera E, Meredith MJ, Summar ML, Smith MD, Voorhees GJ, Stoffel CM, and Freeman ML (1994) Genes regulating glutathione concentrations in X-ray-transformed rat embryo fibroblasts: changes in gamma-glutamylcysteine synthetase and gamma-glutamyltranspeptidase expression. *Carcinogenesis* **15:**1301–1307.

Smyth GK (2004) Linear models and empirical bayes methods for assessing differential expression in microarray experiments. *Stat Appl Genet Mol Biol* **3:**Article 3.

Taniguchi T, Takahashi M, Shinohara F, Sato T, Echigo S, and Rikiishi H (2005) Involvement of NF-kappaB and mitochondrial pathways in docetaxel-induced apoptosis of human oral squamous cell carcinoma. *Int J Mol Med* **15:**667–673.

Tojima Y, Fujimoto A, Delhase M, Chen Y, Hatakeyama S, Nakayama K, Kaneko Y, Nimura Y, Motoyama N, Ikeda K, et al. (2000) NAK is an IkappaB kinase-activating kinase. *Nature* **404:**778–782.

Townsend DM, Tew KD, and Tapiero H (2003) The importance of glutathione in human disease. *Biomed Pharmacother* **57:**145–155.

Urata Y, Yamamoto H, Goto S, Tsushima H, Akazawa S, Yamashita S, Nagataki S, and Kondo T (1996) Long exposure to high glucose concentration impairs the responsive expression of gamma-glutamylcysteine synthetase by interleukin-1beta and tumor necrosis factor-alpha in mouse endothelial cells. *J Biol Chem* **271:**15146–15152.

Varbiro G, Veres B, Gallyas F Jr, and Sumegi B (2001) Direct effect of Taxol on free radical formation and mitochondrial permeability transition. *Free Radic Biol Med* **31:**548–558.

Watson WH and Jones DP (2003) Oxidation of nuclear thioredoxin during oxidative stress. *FEBS Lett* **543:**144–147.

Yang H, Magilnick N, Lee C, Kalmaz D, Ou X, Chan JY, and Lu SC (2005a) Nrf1 and Nrf2 regulate rat glutamate-cysteine ligase catalytic subunit transcription indirectly via NF-kappaB and AP-1. *Mol Cell Biol* **25:**5933–5946.

Yang H, Magilnick N, Ou X, and Lu SC (2005b) Tumour necrosis factor alpha induces co-ordinated activation of rat GSH synthetic enzymes via nuclear factor kappaB and activator protein-1. *Biochem J* **391:**399–408.

Yang H, Wang J, Huang ZZ, Ou X, and Lu SC (2001) Cloning and characterization of the 5′-flanking region of the rat glutamate-cysteine ligase catalytic subunit. *Biochem J* **357:**447–455.

Address correspondence to: Dr. Ying Xia, Department of Environmental Health, College of Medicine, University of Cincinnati, 123 East Shields Street, Cincinnati, OH 45267-0056. E-mail: ying.xia@uc.edu